REVISTA MATÉRIA V.31
ISSN 1517-7076 articles e20260015, 2026

Formation and migration energies of vacancies at the Cu/Ta interface

Viviana Patricia Ramunni[1,2], María Inés Pascuet[2,3], Julián Roberto Fernández[2,3,4]

[1]Comisión Nacional de Energía Atómica, Instituto de Nanociencia y Nanotecnología, Consejo Nacional de Investigaciones Científicas y Técnicas. Av. Gral. Paz, 1499, San Martín, B1650KNA, Buenos Aires, Argentina.

[2]Comisión Nacional de Energía Atómica, Gerencia de Materiales. Av. Gral. Paz, 1499 (1650), San Martín, Argentina.

[3]Consejo Nacional de Investigaciones Científicas y Técnicas. Godoy Cruz, 2290, C1425FDQ, Buenos Aires, Argentina.

[4]Universidad Nacional de San Martín, Instituto Sabato, Comisión Nacional de Energía Atómica. Av. Gral. Paz, 1499, San Martín (1650), Prov. Buenos Aires, Argentina.

e-mail: vpram00@gmail.com, inepascuet@gmail.com, julrfern@gmail.com

ABSTRACT

In this work, we investigate the equilibrium atomic structure of the Cu/Ta interface in the Ta–Cu system, focusing on the Nishiyama–Wasserman orientation relationship, by means of atomistic simulations employing angular-dependent potentials (ADP). Two distinct lattice-mismatch regions, denoted as ZI and ZII, are identified at the interface. The static properties of vacancies and solute–vacancy complexes are systematically analyzed within the first interfacial planes. We find that the vacancy formation energy strongly depends on the local interfacial environment, exhibiting significant variations between ZI and ZII. For solute–vacancy complexes, both binding energies and exchange migration barriers are calculated, revealing noticeable deviations from their corresponding bulk values. Furthermore, the vacancy–solute interaction is found to depend sensitively on the distance from the interface core. In particular, vacancies located on the Ta side act as efficient traps for Cu atoms, promoting an enhanced Cu solubility in the interfacial region. These results provide insight into defect energetics and solute behavior at Cu/Ta interfaces.

Keywords: Ta-Cu; interfaces; solute-vacancy complex; migration; atomistic simulations.

1. INTRODUCTION

Atomistic computer simulations provide valuable insight into the mechanisms governing the stability and mechanical strength of immiscible Cu–Ta alloys, which are of interest for nanocrystalline applications due to their rapid grain growth at elevated temperatures [1, 2]. Cu and Ta adopt FCC and BCC structures, respectively, and exhibit negligible mutual solubility in the solid state [3]. However, mechanical alloying can produce metastable FCC solid solutions in which Ta atoms are incorporated into Cu [4, 5], where solute clustering is believed to contribute to enhanced mechanical properties.

Recent studies on nanoscale metallic multilayers have emphasized the critical role of interfaces in controlling defect evolution, strain distribution, and atomic transport, particularly under irradiation conditions. Experimental and atomistic investigations in systems such as Zr/Nb have revealed a strong asymmetry in defect behavior across interfaces, associated with differences in defect migration barriers and elastic fields [6, 7]. These differences lead to distinct defect accumulation and recovery mechanisms in adjacent layers, highlighting the importance of interface structure in determining material response.

In the Cu–Ta system, most previous atomistic studies have focused on bulk properties and vacancy-mediated diffusion using first-principles methods [8]. These works indicate that interstitial-mediated transport is less relevant due to the high formation energies and low equilibrium concentrations of interstitial defects. However, a detailed atomistic description of defect energetics at Cu/Ta interfaces, particularly accounting for local structural variations, remains limited.

In this work, we present an atomistic study of the Cu/Ta interface based on angular-dependent potentials (ADP) fitted to previuos first-principles based on density functional theory (DFT) and experimental data [1, 2, 9]. We focus on the Nishiyama–Wasserman orientation relationship and identify two structurally distinct interfacial regions (ZI and ZII) arising from lattice mismatch.

Corresponding Author: Viviana Patricia Ramunni Received on: 07/01/2026 Accepted on: 20/05/2026

DOI: https://doi.org/10.1590/1517-7076-RMAT-2026-0015

(cc) BY

Although the interface considered in this work is idealized, it provides a controlled framework to investigate the fundamental atomistic mechanisms governing vacancy behavior at metal interfaces. Such simplified models are widely used to isolate the role of local atomic environments and to extract physically meaningful trends that would otherwise be obscured by structural complexity. The insights obtained here are particularly relevant for understanding defect evolution and void formation in immiscible systems such as Cu–Ta, which are of interest in nanoscale metallic devices. Future work will extend this approach to more realistic, experimentally motivated interface structures and more advanced diffusion descriptions.

Then, we investigate the static properties of vacancies and solute–vacancy complexes in bulk Cu and Ta, as well as in the vicinity of the interface. In particular, we analyze vacancy formation energies, binding energies, and their dependence on the local interfacial environment. Additionally, migration barriers are evaluated to assess possible vacancy-mediated transport mechanisms across the interface.

This work provides insight into the role of interfacial structure in governing defect energetics and solute behavior in Cu/Ta systems, which is relevant for the design of temperature-resistant nanostructured materials.

The remainder of this paper is organized as follows: Section 2 presents our computational methodology, while Section 3 validates the ADP potential developed by PURJA PUN *et al.* [1, 2] through bulk property calculations, and discusses the numerical results for bulk Cu and Ta to assess the potential's accuracy. Section 4 describes the construction of the interface, serving as a prototype for modeling Cu and Ta trapping. In Section 5, we present the formation and binding energies of vacancy-solute complexes within the first atomic planes of the interface core. Also, same section discusses possible vacancy migration pathways in the Cu/Ta system. Finally, the last section summarizes our conclusions.

2. MATERIALS AND METHODS

The static properties were investigated using the molecular statics (MS) technique, implemented in an in-house code named The Monomer method [10], together with angular-dependent (ADP) interatomic potentials for the Cu-Ta system [1]. The Cu-Ta interatomic potential is based on the ADP formalism for Cu and Ta developed by PURJA PUN *et al.* [1, 2, 9]. These potentials provide an accurate description of a wide range of properties of Cu and Ta, including alloys with varying chemical compositions.

Migration is investigated using the Monomer method [10], a static technique designed to explore the potential energy surface and identify saddle-point configurations. The method determines the direction of lowest local curvature relying exclusively on force evaluations. Conceptually, the Monomer approach starts from a local minimum and searches for the saddle points that connect it to neighboring minima.

In practice, the system is driven across the potential energy surface by means of a modified force. This pseudo-force coincides with the conventional downhill force in all directions except one: the component along the eigenvector associated with the lowest curvature is inverted, effectively pushing the system uphill along that direction. As a result, the method converges toward first-order saddle points without requiring explicit Hessian calculations. Owing to this strategy, the Monomer method efficiently identifies the relevant eigenvector using only local force information.

The Ta/Cu interface was constructed following the procedure of SIMONELLI and FERNÁNDEZ [11], and the results are compared with those reported by HEINO [12].

3. THE BULK

First, we evaluated the bulk defect formation properties. Point defect was introduced into a cubic crystallite consisting of several thousand atoms under periodic boundary conditions. The atoms were then allowed to relax in the presence of the defect as vacancies, where the formation energies is computed according to the following expression,

$$E_f^V = E(N-1) - E(N) + \mu \tag{1}$$

In Eq. (1), E ($N-1$) and E (N) are the total energy of the supercell with and without a vacancy (V), and μ is the chemical potential of the atom removed taken as the energy per atom in the bulk $\mu = E(N)/N$. Table 1 summarizes the bulk properties, including the lattice parameters, a_0, and cohesive energies, E_0, of FCC Cu and BCC Ta calculated using the ADP potential [1], in comparison with experimental data and DFT calculations. The characteristics of point defects are also reported, including the vacancy formation energies, E_f^V, vacancy formation entropies, S_f^V, attempt jump frequencies, v_0, and migration energies, E_m^V, obtained using the Monomer method [10], together with the corresponding activation energies.

(cc) BY

Table 1: Bulk properties of FCC Cu and BCC Ta computed with the ADP potential from Ref.[1], in comparison with DFT calculations and experimental data.

FCC CU	ADP	EAM [8]	DFT	EXP.
$a_0\,(\AA)$	3.615	3.615	3.52–3.64 [13]	3.615 [14]
$E_0\,(eV)$	3.540	3.540	3.47–4.15 [13]	3.54 [15]
$E_f^V\,(eV)$	1.272	1.272	1.08–1.30 [13], 1.19 [16]	1.27–1.28 [17]
$E_m^V\,(eV)$	0.689	0.689	0.69 [18]	0.71 [19]
$Q^V\,(eV)$	1.961	1.962		1.98
S_f^V/k_B	1.399	1.404		2.35 [19]
$v_0\,(THz)$	7.60	7.690		
BCC TA	**ADP**	**EAM1 [1]**	**DFT**	**EXP.**
$a_0\,(\AA)$	3.304	3.304	3.36 [20]	3.303 [21]
$E_0\,(eV)$	8.100	8.100		8.1 [14]
$E_f^V\,(eV)$	3.060	2.430	2.99 [22]	3.1 [23]
$E_m^V\,(eV)$	0.820	0.990	0.83 [22]	0.7 [23]
$Q^V\,(eV)$	3.880	3.420	3.98 [23]	3.8 [23]

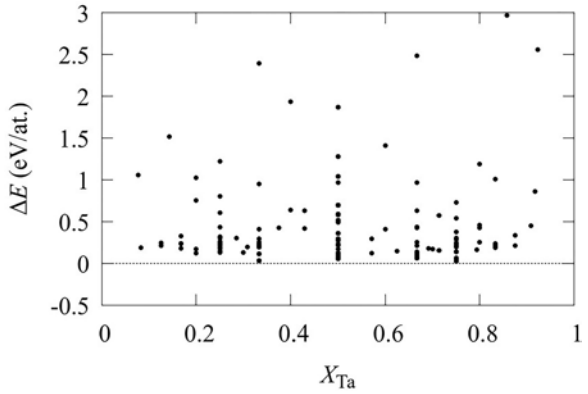

Figure 1: Formation energy per atom ΔE for different Cu-Ta intermetallic structures as a function of X_{Ta}, the atomic fraction of Ta.

Table 1 shows well agreement between EAM [8], EAM1 [1], ADP, DFT, and experimental results. The largest deviation is observed for the BCC Ta vacancy formation energy obtained with the EAM1 potential, relative to experiment and to both DFT and ADP values.

Next, we test the ADP cross-interaction between Cu and Ta by evaluating the formation energy $\Delta E_\alpha = E_\alpha - (1-X_{Ta})\,\mu_{Cu} - X_{Ta}\mu_{Ta}$ of different intermetallic structures, where E_α is the minimized energy per atom of structure α, X_{Ta} the Ta atomic fraction and $\mu_{\mathrm{Cu/Ta}}$ the chemical potentials of each component as defined above. Figure 1 shows the results for around 160 such structures. It must be noted that no negative values of ΔE_α are obtained, suggesting the immiscibility of both components under the ADP model.

Our results are consistent with previously reported values [1], confirming the reliability of the ADP potential in reproducing the bulk and defect properties of FCC Cu and BCC Ta. The agreement with both experimental measurements and DFT calculations provides additional confidence in the accuracy of the present approach.

4. THE INTERFACE

The Nishiyama-Wasswerman (N-W) interface generation method follows a standard computational procedure [11]. Briefly, the interface configuration shown in Figure 2, consists of a Cu/Ta bi-crystalline slab, oriented such that the closest-packed planes and directions of each phase are parallel, i.e., $(111)_{\alpha Cu} \| (001)_{\alpha Ta}$ and $\langle 110\rangle_{\alpha Cu} \| \langle 001\rangle_{\alpha Ta}$.

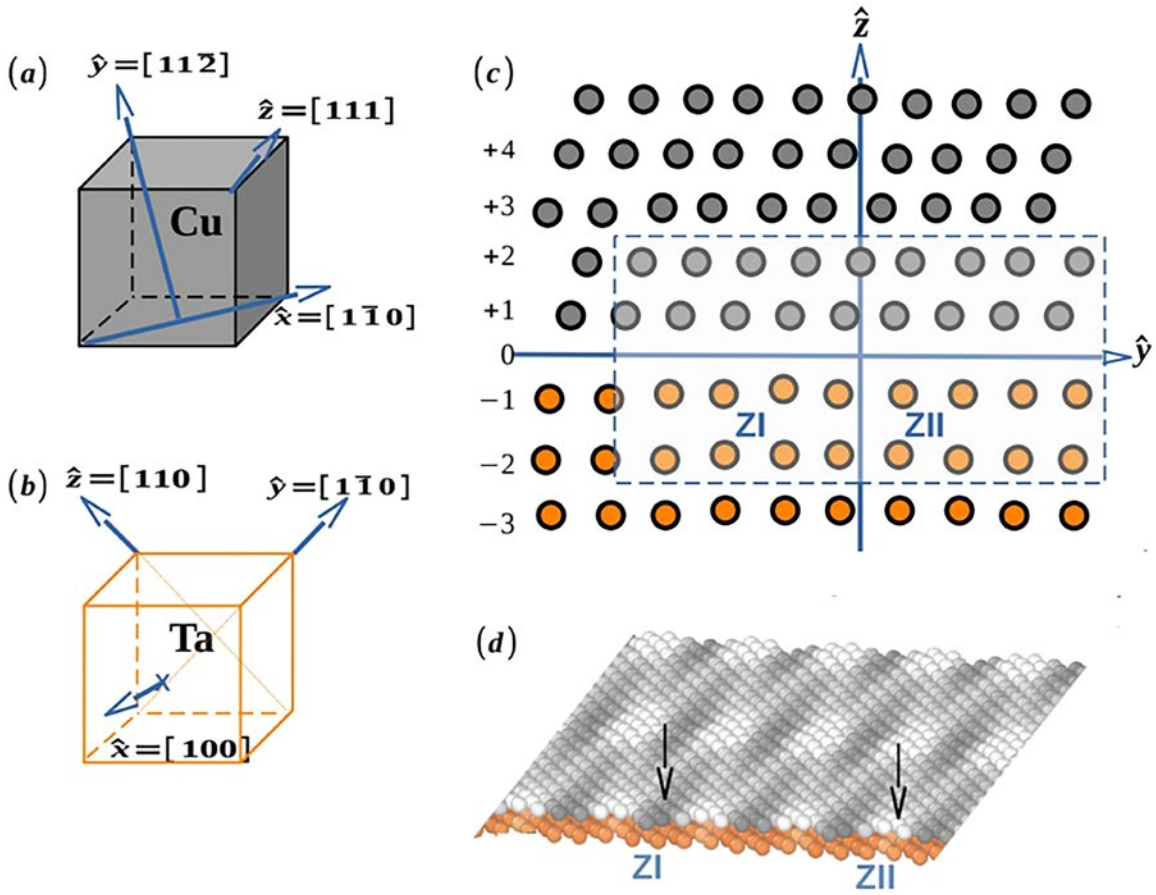

Figure 2: The relaxed Cu/Ta interface structure. The unit cubes on the left indicate the crystallographic axes on both sides: (a) Cu and (b) Ta. In (c), a projection of the interface along the x axis is shown, with the coherent (ZI) and incoherent (ZII) zones labeled. Atomic planes are numbered by an integer n = 0; ±1; ±2; ... Grey (orange) circles correspond to Cu (Ta) atoms. In (d), only the interface core region is represented, with one plane of Cu and one of Ta. Different color shades on atoms at the interface stand for zones of good (ZI) and bad (ZII) lattice mismatch.

Around twenty compact planes are considered for each phase. Atomic positions were relaxed under periodic boundary conditions parallel to the interface plane and free-surface conditions perpendicular to it.

In this system, most interfaces are incommensurable, i.e., the plane dimensions of the two blocks do not perfectly match due to a lack registry between the lattice parameters of the two materials. Under periodic boundary conditions, commensurability is enforced by slightly deforming the structures, which induces a stress field whose magnitude grows with the plane-size mismatch and must be considered when evaluating interface energies. To reduce these effects, block sizes were selected to minimize deviations from commensurability. The simulation block finally contains 23328 Cu and 36656 Ta atoms, with dimensions 92.267 × 79.564 × 73.098 Å^3.

In the relaxed configuration, the energy contribution from the stress field due to the interface plane mismatch, E_σ, increases linearly with the number of planes parallel to the interface. This contribution must be excluded when computing the interfacial energy, E_I. Accordingly, $E(z)$ was calculated as the sum of the energy differences per unit area for all atoms i,

$$E(z) = \sum (E_i + E_0)/A \tag{2}$$

In Eq. (2), A is the interface area, E_i is the energy of atom i with coordinate $z_i < z$ and E_0 is the cohesive energy of the corresponding phase. The atomic layers contributing most to E_I are highly localized at the interface on the Cu side, while they extend slightly further into the Ta phase.

Figure 3 shows an example of the plots employed to compute E_I · E_I is taken as the difference between the values of the lines at z = 0. In general, it is observed that the atomic layers that contribute significantly to E_I are highly localized at the interface in the Ta phase and more extended in the Cu phase.

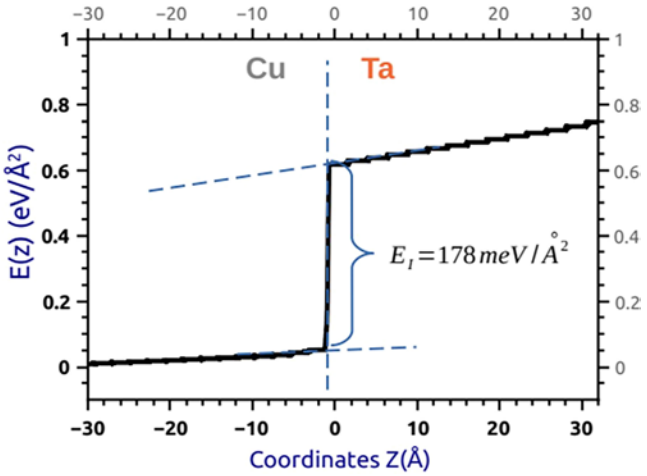

Figure 3: Accumulated energy per unit area and determination of the interfacial energy.

The calculated interfacial energy, E_I = 178 meV/Å², differs from the 131 meV/Å² reported by HEINO [12], although both values are of the same order of magnitude, the difference with our calculated value can be attributed to methodological and modelling choices. Heino used an embedded-atom method (EAM) potential, whereas our calculation employed the ADP potentials [1, 2]. The two results are consistent in magnitude, and the discrepancy is within the expected uncertainty for different modelling approaches.

5. RESULTS

After relaxation, the Ta/Cu interface constructed following the NW orientation exhibits two distinct regions associated with lattice mismatch accommodation referred as coherent (ZI) and incoherent (ZII) zones.

A coherent region (ZI) is characterized by relatively small atomic displacements and reduced local strain, whereas an incoherent region (ZII) exhibits larger structural distortions arising from misfit accommodation. To quantitatively distinguish between coherent (ZI) and incoherent (ZII) interface regions, we analyze the local atomic environment of Cu and Ta atoms in the first interfacial layers.

Figure 4 shows atomic maps of different magnitudes for the first two layers of Cu and Ta close to the NW interface. Cu atoms sitting directly on Ta atoms (shown on Figure 4-a/b as small red circles around the center and top of the figure) correspond to positions with the highest energies and pressures (Figure 4-a/b). After relaxation, those Cu atoms do not move appreciably on the interface plane (shown as blue/green in Figure 4-c) but they instead move away in the perpendicular direction (shown in red in Figure 4-d).

On the other hand, Ta atomic displacements are comparatively much smaller (large blue/green circles in Figures 4-c/d). Cu atoms suffering large relaxations in the *z* direction constitute zones of bad lattice mismatch which will be referred to as ZII zones, in opposition to other zones where lattice mismatch are better, or ZI zones. Atomic positions in zone ZII (high energy and pressure) are expected to bring the lowest vacancy formation energies as this defect will release lattice local pressure.

The Cu side exhibits pronounced site-to-site variations in all three quantities, revealing a highly heterogeneous local environment induced by the interface. In particular, regions associated with ZII display enhanced stress concentrations and larger atomic displacements, while ZI regions remain comparatively uniform. These spatial fluctuations correlate directly with the oscillatory behavior of vacancy formation energies observed in Cu.

In contrast, the Ta side shows a much more homogeneous distribution of local properties, consistent with the nearly constant vacancy energetics in the BCC phase.

In order to extend the analysis beyond bulk properties, point defects were introduced into the ideal NW interface system. In particular, vacancies were generated at selected atomic sites in the vicinity of the interface, allowing us to evaluate their formation and stability in the interfacial environment. The presence of vacancies plays a key role in diffusion-mediated processes and defect interactions in metallic systems. Based on these configurations, solute–vacancy complexes were subsequently constructed by placing Ta (Cu) atoms in substitutional positions adjacent to the vacancy sites. These configurations also provide the basis for constructing solute–vacancy complexes, which are known to significantly influence diffusion mechanisms and segregation behavior. Accordingly, Ta (Cu) atoms were positioned in substitutional sites adjacent to the vacancies, enabling the study of their interaction at the atomic scale.

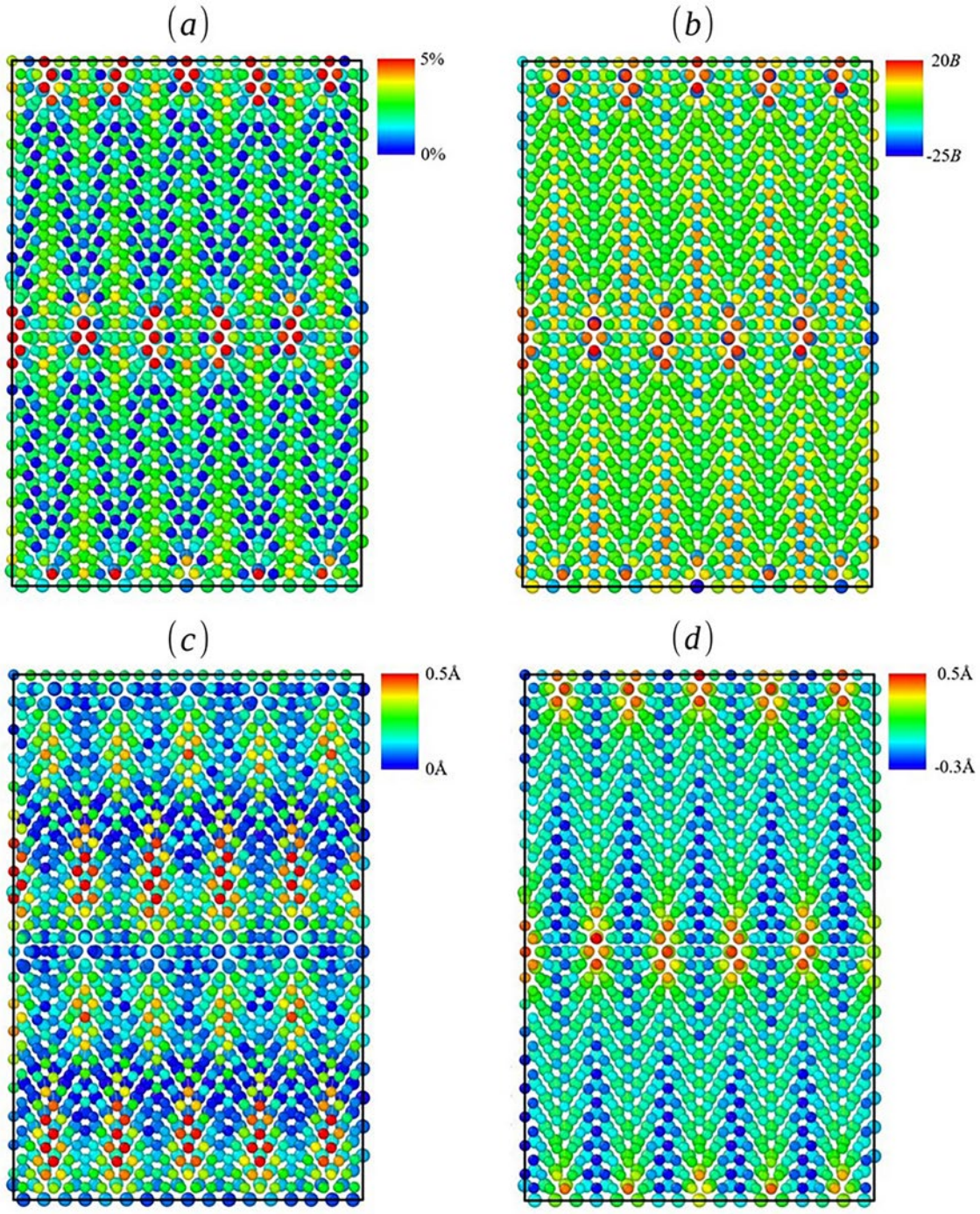

Figure 4: Projections of the relaxed NW interface with atomic maps of different magnitudes for the first layers of Cu (n = 1) and Ta (n = –1): a) potential energies (as a percentage of their respective cohesive energies, 3.54 eV for Cu and 8.1 eV for Ta), b) pressure (as $p = (\sigma_{xx} + \sigma_{yy} + \sigma_{zz})/3$) where σ_{ij} are the stress tensor components, in units of their bulk moduli B, 138.3 GPa for Cu and 194.7 GPa for Ta), c) displacements on the interface plane and d) displacements perpendicular to the interface plane (with respect to the initial atomic positions). Small (large) circles correspond to Cu (Ta) atoms and colors indicating the magnitude of the given value as shown in each scale.

5.1. Segregation

Vacancies can segregate at interfaces, as their formation energies are typically lower than in the bulk, affecting diffusion and interface stability. Vacancies were thus created at different atomic positions within both zones along the perpendicular $\hat{z}$ direction, extending up to about the eleventh layer in each material through ZI and ZII (see Figure 1). Concerning segregation, the energy relative to a reference plane n_∞ (usually a bulk-like position far from the interface) is defined in terms of the vacancy formation energy in Eq. (1) as,

(cc) BY

$$\Delta E(n) = E_f^V(n) - E_f^V(n_\infty) \tag{3}$$

In Eq. (3), a negative value of $\Delta E(n)$ indicates that the vacancy preferentially segregates to plane n relative to the bulk reference, whereas a positive value indicates that segregation is unfavorable. Table 2 lists, in eV, both the vacancy formation energy E_f^V and the segregation energy $\Delta E(n)$, calculated from Eqs. (1) and (3), respectively. Note that in Figure 1, the plane at the center of the Ta/Cu interface is defined as $n = 0$, with the adjacent planes above (Cu) and below (Ta) labeled $n = 1$ and $n = \bar{1}$, respectively. Using this notation, we present our numerical results for the interface.

Formation energies (E_f^V) and segregation energies (ΔE), summarized in Table 2, indicate that E_f^V is positive in both ZI and ZII regions for the Ta and Cu phases. On the Cu side ($n - 1$), the values range from lower (0.664 eV) to higher (1.766 eV) than the vacancy formation energy in bulk Cu (1.272 eV, see Table 1). A similar trend is observed for Ta, particularly at plane $n = \bar{1}$, where both lower (2.085 eV) and higher (3.357 eV) formation energies are obtained compared to bulk Ta (3.06 eV, see Table 1). Concerning segregation, negative values were found on both sides of the interface; on the Cu side at planes $n = 1$ (in ZI), while on the Ta side on plane $n = 1$ (in both ZI and ZII). In Table 2, our ADP calculations show that segregation energies are negative on the first two planes $n = +1$ on both the Ta and Cu sides.

On the Cu side, negative segregation occurs in ZI at $n = 1$, with a minimum energy of −0.608 eV, whereas on the Ta side, negative segregation energies are instead found at $n = 1$ in both ZI and ZII zones. The negative segregation energies observed at the $n = \pm 1$ planes indicate that vacancies preferentially occupy these planes relative to the bulk, whereas the positive values from $n \geq 2$ make these sites less favorable. This energetic preference suggests that vacancies tend to migrate toward the $n = 1$ Cu plane at ZI, thereby promoting Ta diffusion into the Cu region through the vacancy mechanism. Conversely, Cu atoms can migrate at $n = 1$ in both ZI and ZII zones.

The bulk vacancy formation energies for both Cu and Ta are recovered and used as reference values. As expected, Ta exhibits very low, nearly negligible solubility in Cu, and vice versa, reflecting the immiscible character of the system. However, this behavior is modified in the vicinity of the interface core, where vacancy formation energies and solute–vacancy interactions deviate from their bulk values, leading to locally enhanced stability of certain configurations.

The preferential segregation of vacancies to specific interfacial planes can be understood in terms of the local structural and chemical environment [6, 7]. The interface introduces regions of modified atomic coordination and local strain associated with lattice mismatch and structural relaxation. These conditions reduce the energetic cost of vacancy formation relative to the bulk by partially relieving local stress and altering bonding

Table 2: Formation energy, E_f^V, and segregation energy, ΔE, (in eV) calculated in Zone ZI and ZII.

Cu: n − PLANE	E_f^V**(eV) (ZI/ZII)**	ΔE **(eV) (ZI/ZII)**
$n = 1$	0.664/1.766	–0.608/0.494
$n = 2$	1.287/1.455	0.015/0.183
$n = 3$	1.299/1.321	0.027/0.049
$n = 4$	1.326/1.329	0.054/0.057
$n = 5$	1.339/1.347	0.067/0.075
⋮	⋮	⋮
$n = 7$	1.272	~0.0
Ta: n − PLANE	E_f^V**(eV) (ZI/ZII)**	ΔE **(eV) (ZI/ZII)**
$n = \bar{1}$	2.085/3.357	–0.975/–0.703
$n = \bar{2}$	3.099/3.164	0.039/0.104
$n = \bar{3}$	3.216/3.298	0.156/0.238
$n = \bar{4}$	3.216/3.277	0.156/0.217
$n = \bar{5}$	3.224/3.253	0.164/0.193
⋮	⋮	⋮
$n = \bar{7}$	3.060	~0.0

interactions. As a result, vacancies are energetically stabilized at the interface, leading to negative segregation energies. This behavior is consistent with general trends reported in immiscible metallic systems, where interfacial environments provide energetically favorable sites for defect accommodation due to combined strain and coordination effects.

5.2. Migration

In this context, vacancy-mediated diffusion of solute atoms (Ta in Cu and Cu in Ta) is expected to be enhanced near the interface region. To investigate the influence of the local environment on migration, a solute atom was positioned as a first-nearest neighbor to a single vacancy on both sides of the interface. This setup enables a direct comparison between solute and solvent migration barriers.

Additionally, the binding energy between the solute atom and the vacancy, E_B, is computed as:

$$E_B = \left[E(N-1,V)+E(N-1,S)\right]-\left[E(N-2,S)+E(N)\right] \tag{4}$$

where N is the number of solvent atoms, $E(N-1, V)$ and $E(N-1, S)$ are the energies of a crystallite containing $(N-1)$ atoms of solvent plus a vacancy V or a solute atom S, respectively; and $E(N-2, S)$ is the energy of a crystallite containing $(N-2)$ solvent atoms plus one solute atom as the nearest neighbor of a single vacancy. According to the sign convention used here, $E_B > 0$ value means attractive solute-vacancy interaction, whereas $E_B < 0$ means repulsion.

Here, we studied a single vacancy at sites 1 through 7 (see Figure 5) placed at $n = \pm 1$ planes, calculating the vacancy formation energies (summarized in the first column of Table 3) and assessing the stability of each relaxed configuration.

Table 3 summarizes the solute-vacancy exchanges calculated using the Monomer [10]. The first column reports the vacancy formation energy, E_f^V, in the $n = \pm 1$ planes on both sides of the interface, together with the binding energy of solute-vacancy complexes $C_j = S_j - V_{j+1}$, constructed by placing the solute at site j (with j = 1, ..., 7) and the vacancy at its first neighbor j + 1, and translating the pair to cover zones ZI and ZII, as shown in Figure 5. In this figure, on the Ta side, the Cu atom acts as a solute forming the complex $Cu_j - V_{j+1}$, whereas on the Cu side, Ta forms the complex $Ta_j - V_{j+1}$. This figure also illustrates the associated lattice distortions induced by the interface misfit. Furthermore, on each side of the interface we calculated the solvent-vacancy exchange as well as the binding energy of initial and final configurations after vacancy-solute or vacancy-solvent exchange.

In this way, we can study the effects of the lattice mismatch on the vacancy formation energy and on the binding energy of the complex. Figure 6, shows the vacancy formation energy in the first two planes of the interfacial core as a function of the vacancy position (sites 1–7), with the values summarized in the first column of Table 3.

The structural variations are more pronounced on the Cu side of the interface, leading to spatial modulation of vacancy energetic. In contrast, the Ta side exhibits a more uniform local atomic environment, consistent with the weak variation of vacancy energies as shown in Table 2 and Figure 6.

It is worth noting that, along plane $n = 1$ (Cu side), the vacancy formation energy displays an oscillatory behavior across atomic layers, revealing strain-induced relaxations that extend into the Cu region and indicating stronger lattice distortion in the FCC Cu near the interface. In contrast, on plane $n = -1$ (Ta side), the formation energy is nearly uniform, except at one site where the vacancy is unstable.

The structural variations are more pronounced on the Cu side of the interface, leading to a spatial modulation of vacancy energetics. This behavior can be attributed to the higher structural sensitivity of the FCC Cu lattice, where local distortions induced by lattice mismatch and interfacial relaxation produce significant variations in the atomic environment. In contrast, the BCC Ta lattice, characterized by lower packing density and

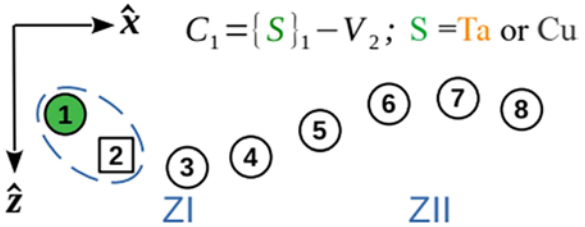

Figure 5: Scheme of complex in planes n = ±1.

Table 3: Formation energies E_f^V, binding energies E_B, and migration energies E_m^V (in eV) of direct/reverse jumps. Binding energies are reported only for the initial/final configurations after solute-vacancy exchange.

$E_f^V(n=\pm1)$	COMPLEX	E_m^V	$E_B\,(C_j)$	CONFIG.
1.272	V-Cu	0.820	0.029	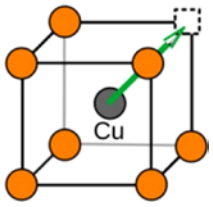
3.060	V-Ta	1.236	–0.658	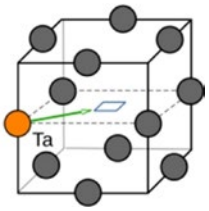
1.299	$C_1 = Ta_1 - V_2$	0.039/0.137	–0.036/0.063	stable
1.418	$C_2 = Ta_2 - V_3$	0.387/0.202	0.179/–0.221	stable
1.403	$C_3 = Ta_3 - V_4$	0.010/0.153	–0.094/0.053	stable
1.659	$C_4 = Ta_4 - V_5$	0.016/0.328	–0.371/–0.059	stable
1.827	$C_5 = Ta_5 - V_6$	0.571/0.531	–0.555/–0.594	stable
1.952	$C_6 = Ta_6 - V_7$	0.358/0.545	–0.618/–0.491	stable
1.915	$C_7 = Ta_7 - V_8$	0.447/0.126	0.731/0.417	stable
2.481	$C_1 = Cu_1 - V_2$	Figure 5		Unst.
2.559	$C_2 = Cu_2 - V_3$	0.118/0.286	–0.875/–1.043	stable
2.571	$C_3 = Cu_3 - V_4$	Figure 6		Unst.
2.549	$C_4 = Cu_4 - V_5$	Figure 7		stable
2.485	$C_5 = Cu_5 - V_6$	0.305/0.288	–1.063/–1.140	stable
2.494	$C_6 = Cu_6 - V_7$	0.324/0.436	–1.041/–1.154	stable
2.508	$C_7 = Cu_7 - V_8$	no exch.	–0.929	stable

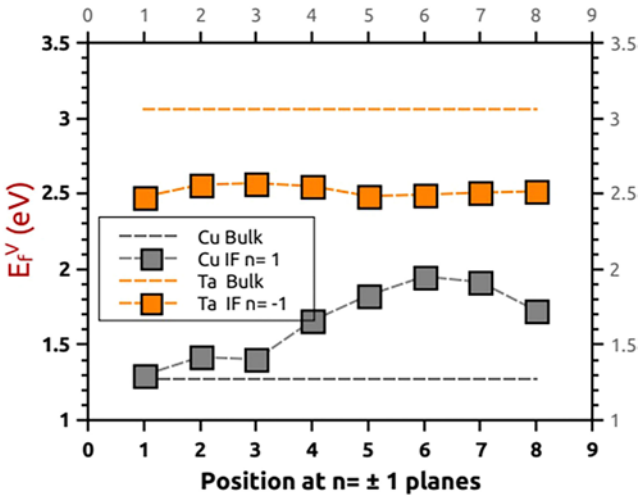

Figure 6: Vacancy formation energy (in eV) within n = 1 and n = –1 planes within the interface core region in terms of atomic position along x-axis.

higher mechanical stiffness, accommodates interfacial strain more uniformly. As a result, the local atomic environment on the Ta side remains closer to its bulk configuration, consistent with the weaker variation observed in vacancy formation energies.

Table 3 summarizes the solute–vacancy exchange processes. On the Cu side, all complexes are stable, with migration consistently occurring between Ta atoms and the vacancy. On the Ta side, most complexes are also stable, except for two cases where negative binding energies between Cu and the vacancy indicate instability.

Here, a configuration is classified as unstable when structural relaxation leads to dissociation of the initial vacancy–solute complex and convergence to a different atomic configuration. Such behavior is generally associated with negative binding energies, indicating an energetically unfavorable interaction between the defects.

Other jumps involving solvent atoms and a vacancy are summarized in Figures 7 to 11. These figures present the solvent-vacancy exchange migration barriers for direct and reverse jumps between initial and final configurations, together with their corresponding binding energies E_B (in blue), calculated from Eq. (4).

Figure 7 shows in panel (a) the initial complex configuration $C_1 = Cu_1 - V_2$, which becomes unstable after relaxation. The relaxed state corresponds to a delocalized vacancy in the $n = \pm\bar{1}$ planes, with a Cu atom at the center (b). Two saddle points connect this state to distinct final configurations: (c) Cu labeled 2 (d) migrates to $n = \bar{1}$, yielding two Cu atoms at $n = \bar{1}$ (Ta side) and a vacancy at $n = 1$ (0.001/0.032 eV forward/reverse); and (b) a multiple-jump involving three atoms of Cu labeled 1, 2 and 3 with a direct/reverse migration barriers of 0.093/0.549 eV.

Figure 8(a) shows the $C_3 = Cu_3 - V_4$, complex configuration. After relaxation, Cu(2) occupies the vacancy at $n = \bar{1}$, leaving one at $n = 1$ (Cu side). Unlike the delocalized vacancy obtained in Figure 7, this relaxed state is localized, and Cu (3) at $n = 1$ exchanges with the vacancy in the same plane, with migration barriers of 0.132/0.753 eV (forward/reverse).

In the complex $C_4 = Cu_4 - V_5$, no solute-vacancy exchanges were observed. However, two Ta-mediated transitions were identified, exhibiting migration barriers of 0.038/0.599 eV and 0.038/0.456 eV for the forward and reverse jumps, respectively (Figure 9-a/b). These transitions correspond either to the migration of a single Ta atom (labeled 2) along the x direction, or to a collective jump within the xy plane involving two Ta atoms (labeled 3 and 4).

Figures 10(a) and (b) panels show the complex $C_5 = Cu_5 - V_6$, in which two distinct transitions were identified: (a) the migration of Ta (2) into the vacancy site, with migration barriers of 0.083/0.555 eV, and (b) a solute-vacancy exchange, with migration barriers of 0.228/0.305 eV.

The $C_6 = Cu_6 - V_7$ complex, also located in zone ZII, exhibits similar behavior. Two distinct transitions are identified: (1) a Cu-vacancy exchange with migration barriers of 0.324/0.436 eV, and (2) migration of a solvent atom (Ta) into the V 7 site with 0.010/0.496 eV. These processes are illustrated in Figures 11(a) and (b).

Figures 10 and 11 allow a comparison of solute and solvent jumps toward the vacancy site. In jump (a) of both figures, the solvent atom Ta (2) migrates with a barrier roughly an order of magnitude lower than that of the solute-vacancy exchange in jumps (b). In Figure 11 (a), the jump left the vacancy away from the solute, whereas

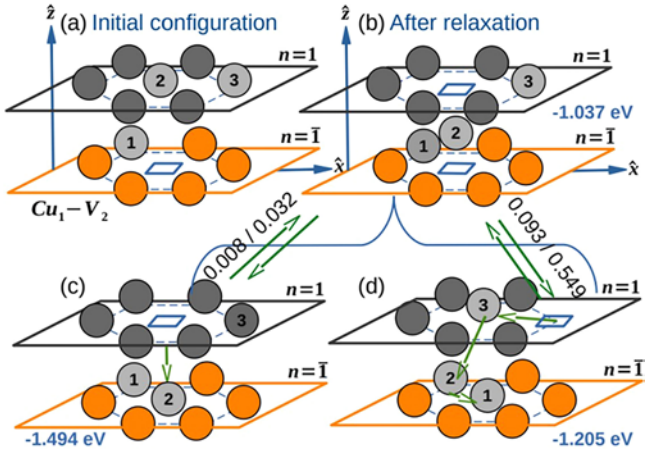

Figure 7: (a) Unstable initial configuration. (b) Relaxed configuration of the solute-vacancy complex, $Cu_1 - V_2$. (c) Schematic of a single Cu jump (atom labeled 2). (d) Schematic of a concerted three-atom jump involving atoms 1, 2 and 3. Arrows indicate direct/reverse atomic jumps.

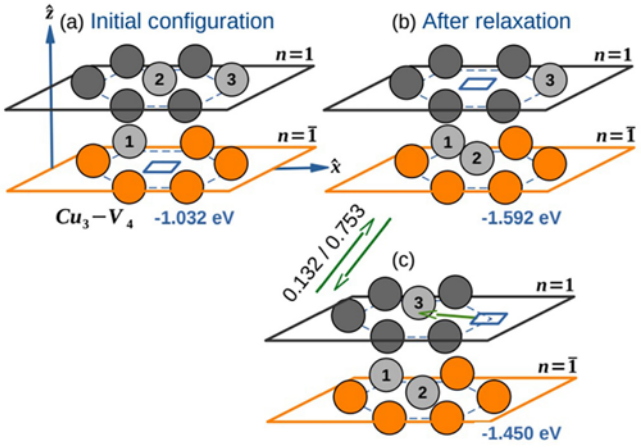

Figure 8: (a) Unstable initial configuration. (b) Relaxed configuration of the solute-vacancy complex $Cu_3 - V_4$. (c) Migration of the Cu atom labeled 3 into the vacancy site located in the $n = 1$ plane on the Cu side.

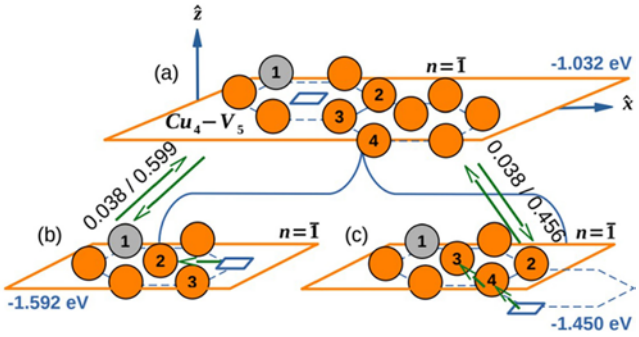

Figure 9: (a) Stable initial configuration of the $Cu_4 - V_5$ complex. Two jumps involving (b) one Ta atom labeled 2 and (c) a cooperative migration of two Ta atoms labeled 3 and 4 within the $n = \bar{1}$ plane on the Ta side.

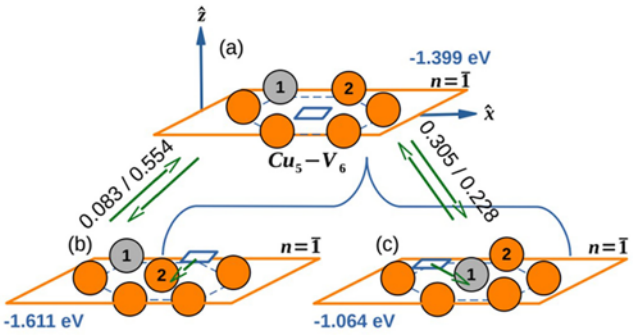

Figure 10: (a) Relaxed configuration of the $C_5 = Cu_5 - V_6$ complex. (b) Migration jump involving a single Ta atom (solvent). (c) Migration of a Cu atom (solute). Both jumps (b) y (c) occuring in the n – 1 plane of the BCC Ta side.

in Figure 10, the vacancy remains a first neighbor to the solute after exchanging with Ta (2). In summary, a wide range of migration barrier values is observed, which can be attributed to atomic mismatch effects within the core region of the interface, where the two crystals join. Another observation is that, on the Cu side in zone ZII, vacancy segregation is favorable and can lead to the trapping of Ta atoms within the interfacial core, but only at specific sites forming preferential pathways of contiguous Ta atoms (hereafter referred to as “Ta channels”). In the next section, we focus on solute atom jumps, either Ta or Cu, that cross the interface from $n = 1$ to $n = \bar{1}$ or vice-versa.

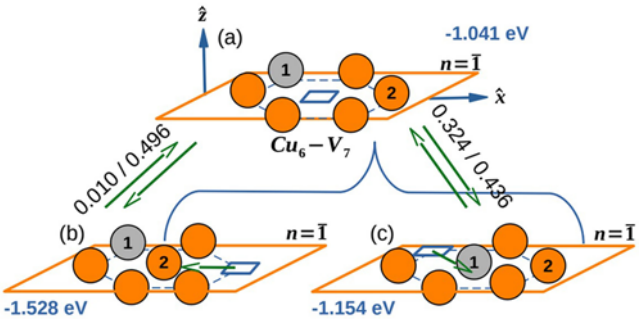

Figure 11: (a) Relaxed complex configuration $Cu_6 - V_7$, (b) Ta (solvent) and (c) Cu (solute) migration within $n = \bar{1}$ at BCC Ta side.

Cooperative multi-atom jumps, such as the mechanisms illustrated in Figure 7(d) and Figure 9(c), corresponding to Cu and Ta solvent atom migration, are indeed intriguing and may become relevant at finite temperature. Their contribution is primarily governed by the associated activation energies. In the present case, the mechanism involves the displacement of two Cu/Ta atoms and can be interpreted as two coupled atomic jumps rather than a fully concerted motion, emerging as a viable minimum energy pathway within the distorted interfacial environment. As interfaces such as Cu/Ta, are characterized by significant lattice mismatch and local strain, can facilitate correlated atomic rearrangements that are unlikely in bulk systems.

Although the dimer method identifies this mechanism as an energetically accessible transition path, it does not provide direct information on its statistical weight. Therefore, while the existence of such cooperative jumps suggests that they may contribute to diffusion under certain conditions, their actual relevance at finite temperature would require further assessment, for instance through kinetic Monte Carlo or molecular dynamics simulations.

It is worth noting that the migration barriers associated with this mechanism are comparable to those of single-atom vacancy jumps. Moreover, the forward migration barrier is significantly lower than the reverse one, indicating an asymmetric energy landscape along this pathway.

The calculated vacancy formation tendencies and migration barriers provide the atomistic energetic parameters that ultimately control macroscopic diffusion behavior. The results indicate that the interfacial region exhibits a heterogeneous energy landscape, where defect transport is expected to be spatially non-uniform. Regions characterized by enhanced vacancy stability and reduced migration barriers are likely to act as preferential pathways for vacancy-mediated transport, whereas regions associated with higher local strain and larger activation energies are expected to hinder defect motion. Consequently, the interface is predicted to function as a spatially selective transport pathway. A quantitative evaluation of macroscopic diffusion coefficients would require finite-temperature simulations and kinetic modeling, which are beyond the scope of the present work.

Finally, our findings indicate that the minimum-energy configuration corresponds to a delocalized vacancy that can adopt two distinct arrangements: (i) two vacancies in the n = ±1 planes with a Cu atom at the center, and (ii) a similar configuration with a Ta atom at the middle. Among the various possible migration pathways within the interface, we propose one that connects these two configurations as shown in Figure 12. This delocalized vacancy configuration is taken as the starting point for the search of saddle points. We start from a delocalized vacancy between $n = \pm 1$, with a Cu atom located at the center of both planes (C_0 in Figure 10(a)). The Cu atom migrates toward one of the vacancies at $n = \bar{1}$, leaving behind a vacancy at $n = 1$, corresponding to the final configuration C_f, which involves two Cu atoms (labeled 1 and 2). From this final configuration, we perform a new saddle point search, resulting in a Ta jump (labeled 3) from $n = \bar{1}$ toward $n = 1$. This analysis reveals that Ta again forms a delocalized vacancy configuration, now with the Ta atom at the center. Both configurations, (1) and (2), with either Cu or Ta at the center of the two vacancies at $n = 1$ and $n = \bar{1}$, are also connected by a direct jump, as illustrated in Figure 11(b). In Figure 12, we show how configurations (C_0) and (C_f) are connected through the migration steps indicated by green arrows. We have also identified other stable configurations with higher formation energies than (C_0) and (C_f), which migrate along the x and y directions on the $n = \pm 1$ planes, with migration barriers around 0.7 and 0.8 eV close to that obtained for the bulk of fcc Cu and bcc Ta, respectively.

Based on the results presented in Table 3, we propose a solute Ta migration pathway driven by a vacancy mechanism within the interface core from ZI to ZII. Figures 11 (a) and (b) summarize the migration

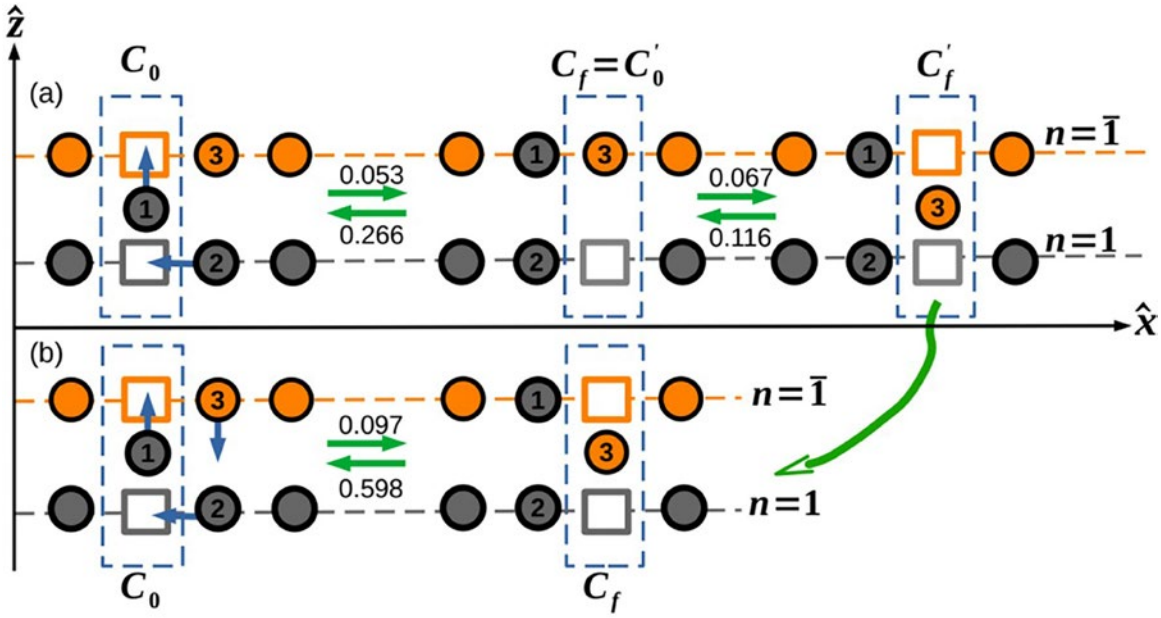

Figure 12: Schematic representation of delocalized vacancy migration pathways in $\hat{x}$.

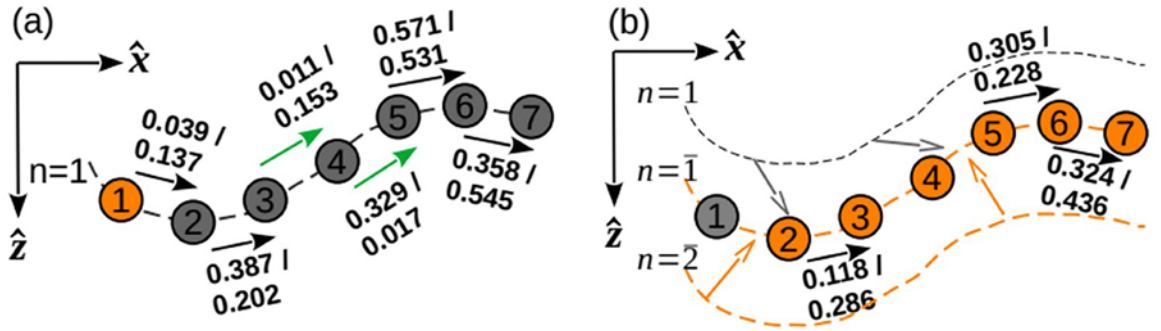

Figure 13: Ta (a) and Cu (b) migration within $n = \pm 1$ planes driven by vacancies, respectively. In (b), grey and orange arrows represent Cu and Ta jumps toward the vacancy at $n = -1$, from $n = 1$ and $n = \bar{2}$, respectively.

energies of (a) Ta-solute atoms driven by vacancies along the $n = 1$ of the Cu side and (b) Cu migration in Ta ($n = \bar{1}$), respectively.

In Figure 13(a), Ta-vacancy exchanges within the $n = 1$ plane are indicated by black and green arrows. The green arrows correspond to jumps between zones ZI and ZII, defining a transition region centered on the site labeled as 4. In contrast, for Cu in Ta, only three possible solute–vacancy exchanges were found, with the most probable being the exchange of the vacancy in the $n = -1$ complex with atoms located in the $n = 1$ and $n = \bar{2}$ planes, as shown by the green and orange arrows in Figure 13(b). This case will be explored in more detail in a forthcoming study, where we will show that Cu migration in Ta proceeds through jumps to the $n = 1$ plane in the Cu phase, promoting Cu motion toward the $n = \bar{1}$ plane. Also in Figure.13, grey and orange arrows correspond to Cu and Ta jumps towards the vacancy forming the complex at $n = \bar{1}$, from $n = 1$ and $n = \bar{2}$, respectively. This type of jumps will be studied in an upcoming paper.

The vacancy-solute complexes in the bcc Ta region ($z < 0$) can be stabilized in certain areas within zones ZI, ZII, and their transition region. In other cases, relaxation drives the vacancy toward the Cu side, leaving two Cu atoms on the Ta side that repel the vacancy. Some regions enable facile Cu migration within Ta, whereas in others, Cu remains immobile and solvent migration becomes dominant. The combination of low forward/reverse migration barriers for solvent jumps and higher forward/reverse barriers for solute motion highlights the complexity of the energy landscape and the asymmetric defect mobility across the interface.

(cc) BY

The present study focuses on migration energetics and atomistic transport pathways at the Cu/Ta interface. The preferential stabilization of vacancies and the identification of energetically favorable migration pathways near the $n = \pm 1$ interfacial planes indicate that atomic transport is spatially localized at specific regions of the interface. These results provide the atomistic foundation required for the future determination of effective diffusion coefficients and their comparison with experimental interfacial diffusion behavior. A comprehensive analysis of diffusion processes and their macroscopic implications is beyond the scope of the present work and will be addressed in a forthcoming study. In this context, the present results represent a step forward in the atomistic investigation of metal/metal interfaces using ADP interatomic potentials, which will be extended to more complex and realistic interfacial configurations in future work.

In summary, the spatial variation of vacancy formation energies and migration barriers observed at the Cu/Ta interface can be interpreted in terms of heterogeneous local strain arising from lattice mismatch accommodation. Such strain-mediated modifications of defect energetics have been widely reported in heterogeneous and multilayer systems, where local structural distortions influence defect stability, migration pathways, and sink efficiency [7,8]. In the present system, we have demonstrated that the coexistence of structurally distinct interfacial regions produces a non-uniform local environment that modulates both vacancy stability and binding energies. These results support the general view that defect energetics at metal/metal interfaces are governed primarily by local structural and stress fields.

The trends observed in this work are consistent with recent atomistic and experimental studies on metallic interfaces, which highlight the dominant role of the local atomic environment in governing defect energetics and diffusion behavior. In particular, the strong dependence of vacancy formation energies on the interfacial region (ZI vs. ZII) reflects the heterogeneous energetic landscape typically reported for immiscible interfaces, where local coordination and structural features give rise to spatially varying defect stability.

Similar behavior has been reported in Zr/Nb multilayers, where interfaces act as active regions for defect absorption and significantly modify the local strain and defect distribution, behaving as efficient sinks for irradiation-induced defects [24]. These findings support the interpretation that the interface is not a passive boundary, but rather a region with distinct thermodynamic and kinetic properties.

Furthermore, the preferential trapping of Cu atoms by vacancies on the Ta side of the interface is in line with previous studies showing that defect–solute interactions are strongly enhanced at interfaces, leading to local deviations from bulk solubility and to non-uniform segregation patterns. Recent atomistic works have emphasized that such behavior originates from the interplay between lattice mismatch, chemical interactions, and local atomic coordination, which together define energetically favorable trapping sites and diffusion pathways.

In this context, the identification of specific regions within ZII that promote vacancy segregation and solute trapping suggests the emergence of preferential migration pathways, consistent with the concept of localized diffusion channels reported in complex metallic interfaces.

Overall, these results reinforce the general picture that interfaces in immiscible systems exhibit highly heterogeneous energetic and kinetic landscapes, where defect stability, segregation, and migration are controlled by the local atomic structure rather than by bulk properties alone.

6. CONCLUSION

In this work, we have analyzed vacancy formation, segregation, and migration energies, as well as the binding energies of vacancy-solute complexes, both in the bulk and at the Cu/Ta interface. The interface was examined in two distinct regions, ZI and ZII, where lattice mismatch occurs. Preliminary migration calculations reveal how vacancies and vacancy-mediated solute exchanges respond to the local environment on both the Cu and Ta sides. Overall, our results show that vacancy behavior at the interface is strongly region-dependent, with solutes generally stabilizing delocalized vacancies in the $n = \pm 1$ planes at the interface core. These findings highlight the crucial influence of the fcc-bcc lattice mismatch on vacancy energetics and provide a solid foundation for future studies of mechanical and transport properties in Cu-Ta nanostructures. In addition, we have demonstrated the reliability of the Cu-Ta ADP potential in modeling the structural and energetic properties of Cu-Ta systems. Finally, this study represents a first step toward a comprehensive understanding of point defects at the Ta/Cu interface, focusing here on vacancies.

Vacancy energetics correlate with spatial variations in local atomic volume induced by mismatch accommodation. Concerning migration we have observed that saddle points are sensitive to the local stress state through changes in the activation volume associated with atomic transport.

Future work will extend the present framework by explicitly incorporating vacancy and solute diffusion, allowing direct comparison with experimentally observed defect transport and accumulation phenomena.

In particular, the combination of atomistic simulations and experimental techniques such as positron annihilation spectroscopy and nanoindentation will provide a comprehensive understanding of the interplay between interface structure, defect dynamics, and macroscopic material response.

7. ACKNOWLEDGMENTS

Authors acknowledge PIP-2021 CONICET 11220200100318CO for partial support.

8. DATA AVAILABILITY

The datasets generated and analyzed during the current study are available from the corresponding author upon reasonable request.

9. BIBLIOGRAPHY

[1] PURJA PUN, G.P., DARLING, K.A., KECSKES, L.J., *et al*., "Angular-dependent interatomic potential for the Cu-Ta system and its applica-tion to structural stability of nano-crystalline alloys", *Acta Materialia*, v. 100, pp. 377–391, 2015. doi: https://doi.org/10.1016/j.actamat.2015.08.052.

[2] MISHIN, Y., LOZOVOI, A.Y., "Angular-dependent interatomic potential for tantalum", *Acta Materialia*, v. 54, n. 19, pp. 5013–5026, 2006. doi: https://doi.org/10.1016/j.actamat.2006.06.034.

[3] MASSALSKI, T.B. *Binary Alloy Phase Diagrams*, Materials Park, OH, ASM, 1986.

[4] FROLOV, T., DARLING, K.A., KECSKES, L.J., *et al*., "Stabilization and strengthening of nanocrystalline copper by alloying with tantalum", *Acta Materialia*, v. 60, n. 5, pp. 2158–2168, 2012. doi: https://doi.org/10.1016/j.actamat.2012.01.011.

[5] DARLING, K.A., ROBERTS, A.J., MISHIN, Y., *et al*., "Grain size stabilization of nanocrystalline copper at high temperatures by alloying with tantalum", *Journal of Alloys and Compounds*, v. 573, pp. 142–150, 2013. doi: https://doi.org/10.1016/j.jallcom.2013.03.177.

[6] ZHAO, Y., LU, G., "First-principles simulations of copper diffusion in tantalum and tantalum nitride", *Physical Review B: Condensed Matter and Materials Physics*, v. 79, n. 21, pp. 214104, 2009. doi: https://doi.org/10.1103/PhysRevB.79.214104.

[7] DAGHBOUJ, N., SEN, H.S., BENSALEM, M., *et al*., "Asymmetrical defect sink behavior of HCP/BCC Zr/Nb multilayer interfaces: bubble-denuded zones at Nb layers", *Acta Materialia*, v. 301, pp. 121579, 2025. doi: https://doi.org/10.1016/j.actamat.2025.121579.

[8] DAGHBOUJ, N., SEN, H.S., ČÍŽEK, J., *et al*., "Characterizing heavy ions-irradiated Zr/Nb: Structure and mechanical properties", *Materials & Design*, v. 219, pp. 110732, 2022. doi: https://doi.org/10.1016/j.matdes.2022.110732.

[9] MISHIN, Y., MEHL, M.J., PAPACONSTANTOPOULOS, D.A., *et al*., "Structural stability and lattice defects in copper: ab initio, tight-binding and embedded-atom calculations", *Physical Review B: Condensed Matter*, v. 63, n. 22, pp. 224106, 2001. doi: https://doi.org/10.1103/PhysRevB.63.224106.

[10] RAMUNNI, V.P., ALURRALDE, M.A., PASIANOT, R.C., "Search of point defect transition states in hcp twin boundaries: the monomer method", *Physical Review B: Condensed Matter and Materials Physics*, v. 74, n. 5, pp. 054113, 2006. doi: https://doi.org/10.1103/PhysRevB.74.054113.

[11] SIMONELLI, G., FERNÁNDEZ, J.R., "Atomistic study of the Zr(HCP)/Nb(BCC) interface", In: *ANALES AFA21*, pp. 183–186, Rosario, 2009.

[12] HEINO, P., "Microstructure and shear strength of a Cu-Ta interface", *Computational Materials Science*, v. 20, n. 2, pp. 157–167, 2001. doi: https://doi.org/10.1016/S0927-0256(00)00173-7.

[13] MEDASANI, B., HARANCZYK, M., CANNING, A., *et al*., "Vacancy formation energies in metals: a comparison of MetaGGA with LDA and GGA exchange-correlation functionals", *Computational Materials Science*, v. 101, pp. 96–107, 2015. doi: https://doi.org/10.1016/j.commatsci.2015.01.018.

[14] KITTEL, C., *Introduction to Sold State Physics*, New York, Wiley-Interscience, 1986.

[15] SMITH, C. J., *Metal Reference Book*, 5th ed., London, Butter-worth, 1976.

[16] CHENG, Y.X., ZHU, L., WANG, G., *et al*., "Vacancy formation energy and its connection with bonding environment in solid: a high-throughput calculation and machine learning study", *Computational Materials Science*, v. 183, pp. 109803, 2020. doi: https://doi.org/10.1016/j.commatsci.2020.109803.

[17] SIEGEL, R.W., "Vacancy concentrations in metals", *Journal of Nuclear Materials*, v. 69-70, pp. 117–146, 1978. doi: https://doi.org/10.1016/0022-3115(78)90240-4.

(cc) BY

[18] MARTÍNEZ, E., UBERUAGA, B.P., "Mobility and coalescence of stacking fault tetrahedra in Cu", *Scientific Reports*, v. 5, n. 1, pp. 9084, 2015. doi: https://doi.org/10.1038/srep09084. PubMed PMID: 25765711.

[19] BALLUFFI, R.W., "Vacancy defect mobilities and binding energies obtained from annealing studies", *Journal of Nuclear Materials*, v. 69-70, pp. 240–263, 1978. doi: https://doi.org/10.1016/0022-3115(78)90247-7.

[20] BERCEGEAY, C., BERNARD, S., "First-principles equations of state and elastic properties of seven metals", *Physical Review B: Condensed Matter and Materials Physics*, v. 72, n. 21, pp. 214101, 2005. doi: https://doi.org/10.1103/PhysRevB.72.214101.

[21] DEWAELE, A., LOUBEYRE, P., MEZOUAR, M., "Refinement of the equation of state of tantalum", *Physical Review B: Condensed Matter and Materials Physics*, v. 69, n. 9, pp. 092106, 2004. doi: https://doi.org/10.1103/PhysRevB.69.092106.

[22] SATTA, A., WILLAIME, F., DE GIRONCOLI, S., "Characterisation of lattice damage formation in tantalum irradiated at variable temperatures", *Phys. Rev B.*, v. 60, pp. 7001–7005, 1999. doi: https://doi.org/10.1103/PhysRevB.60.7001.

[23] EHRHART, P., JUNG, P., SCHULTZ, H., et al., "Atomic defects in metals", In: H. Ullmaier (ed), Landolt Börnstein: New Series Group III: Crystal and Solid State Physics, Berlin, Springer-Verlag, pp. 161–172, 1991.

[24] SEN, H.S., DAGHBOUJ, N., CALLISTI, M., *et al*., "Interface-driven strain in heavy ion-irradiates Zr/Nb nanoscale metallic multilayers: Validation of distortion modeling via local strain mapping", *ACS Applied Materials & Interfaces*, v. 14, n. 10, pp. 12777–12796, 2022. doi: https://doi.org/10.1021/acsami.1c22995. PubMed PMID: 35235286.